EXPERIMENTAL AND NUMERICAL ANALYSIS OF A MOORED FLOATING STRUCTURE RESPONSE TO WAVES

D. Dessi, A. Carcaterra, G. Diodati
INSEAN, DIMA - University of Rome "La Sapienza", CIRA
d.dessi@ insean, antonio.carcaterra@uniroma1.it, g.diodati@cira.it

1. INTRODUCTION

The response of a complex structure undergoing wave forces in regular and irregular sea is investigated. A set of experiments are performed in a towing tank basin (INSEAN) provided with a wave maker. The analysis is carried on by considering the configuration of three bodies of rectangular transverse section and planform coupled together by elastic cables and individually moored to the seabed. This configuration is actually used in special docking operation for ships and submarines as well. The prediction of the wave loads is of practical importance, both to preserve the structural safety of the system (and of the mooring lines) and to avoid dangerous collisions between the floating structure and the docked vessels (see, for instance, Inoue [1] and Ansari [2]). The design of this system presents several difficulties due to the complexity of the analysed structure. This justifies the development of numerical simulations able to predict the whole system response (rigid-body motion and mooring-chain forces) and their validation through direct experimental measurements. Only selected cases in regular and irregular waves are presented in this paper.

2. EXPERIMENTAL SET-UP

The physical system under investigation is constituted by three floating bodies of the same size whose shape and principal dimensions are shown in Fig. 1. In order to reproduce a more realistic configuration of the cables, an artificial seabed providing constant water depth ($h = 0.50\ m$) was laid with metallic nets attached to a truss in the INSEAN towing tank basin. In Fig. 1 the fenders, the linking cables connecting adjacent pontoons, and the mooring lines are displayed. The fenders, of semi-cylindrical shape, were dressed of rubber, whereas the metallic linking cables are made of steel. The connection points of the mooring lines were inserted on the lower wetted face close to the vertices. All the cables used for mooring are built with metallic chains and were fixed on the artificial seabed through two ballasts. In Fig. 2 the actual configuration of the three floating bodies, connected to each other with cables and moored to the sea bed with eight lines, is shown. The overall length is about 4 m. The side mooring lines are connected to the intermediate pontoon (n.2), whereas the bow and stern mooring lines are connected to the first (n.1) pontoon and to the last one (n.3), respectively. In the following, we assume that the waves travel from the pontoon n.1 to the pontoon n.3, as indicated by the white arrow. The rigid body motions of pontoons are recorded using the Krypton Rodym DMM system (based on cameras sensing LEDs glued on-board), the MOTAN system (an inertial motion sensor unit), and some inclinometers and accelerometers. The measurement of the mooring-line forces is obtained by water-proof load cells, each one connected to the model with a spherical linkage allowing the cell to follow the direction assumed by the chain.

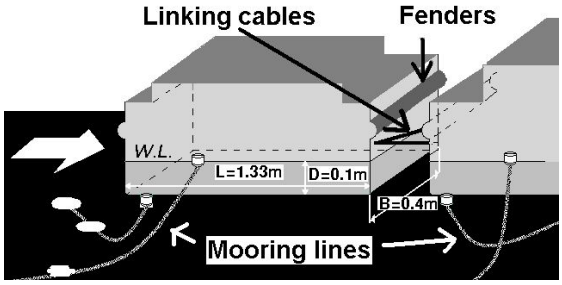

Figure 1: Configuration of the floating structure.

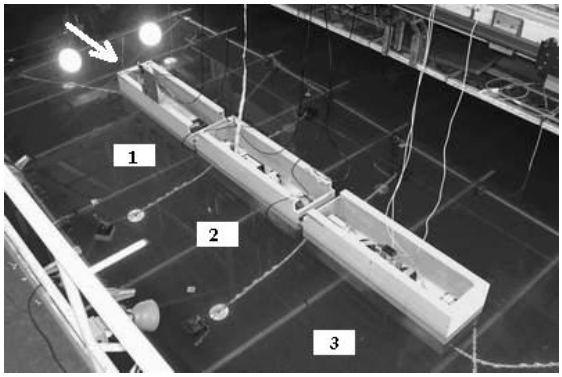

Figure 2: Experimental set-up.

3. MODELING THE FLOATING STRUCTURE

The mathematical model for the single floating pontoon is introduced. Each pontoon is regarded as a rigid body with six dof. Two co-ordinate systems are used for describing the body motion: an inertial Cartesian co-ordinate system (XYZ) fixed to the basin floor (the $X-Y$ plane concides with the still water level), and a body co-ordinate system (xyz) with origin G, the center of gravity of the pontoon. At time $t = 0$ the reference system (XYZ) coincides with the body-fixed co-ordinate system (xyz).
The equations of motion of a single rigid body are:

$$M\dot{\mathbf{v}}_G = \mathbf{f}, \quad (\mathbf{J}\dot{\boldsymbol{\omega}}) = \mathbf{m}, \quad \dot{\mathbf{x}} = \mathbf{v}_G, \quad \dot{\mathbf{R}} = \boldsymbol{\Omega}^T\mathbf{R}, \qquad (1)$$

where $\mathbf{x}_G = \{x_G, y_G, z_G\}^T$ and $\mathbf{v}_G$ are the co-ordinate vector and the velocity vector of G, respectively, M the body's mass, $\mathbf{J} = \mathbf{R}\mathbf{J}_b\mathbf{R}^T$ the inertia tensor, with $\mathbf{J}_b = diag\{J_{xx}, J_{yy}, J_{zz}\}^T$, $\boldsymbol{\omega} = \{\omega_x, \omega_y, \omega_z\}^T$ the angular velocity vector, $\mathbf{R}$ is the orthogonal rotation ma-

trix, $\mathbf{\Omega}$ the angular velocity anti-symmetric matrix, $\mathbf{f}$ the external force, $\mathbf{m}$ the external moment. It should be noted the total number of variables is eighteen, because the matrix $\mathbf{R}$ has nine elements. However, since they are not independent, one can reduce the number of variables to twelve (six generalized displacements and six generalized velocities) by using the Euler angles $\boldsymbol{\alpha} = \{\varphi, \theta, \psi\}^T$. The second of Eq. 1 in the reference system (xyz) is:

$\dot{\omega}_i = \omega_{i+1}\omega_{i+2}(J_{i+1,i+1} - J_{i+2,i+2})/J_{ii} + m_i/J_{ii}$

where $i = x, y, z$, that, using $\boldsymbol{\alpha}$, becomes $\mathbf{A}\ddot{\boldsymbol{\alpha}} + \mathbf{b} = \mathbf{m}$, where the expressions of the matrix $\mathbf{A}$ and of the vector $\mathbf{b}$ (both depending on $\boldsymbol{\alpha}$) are not given for sake of conciseness. This procedure presents some numerical difficulties since the system might be numerically unstable due to singularities in the $\mathbf{A}$ matrix. An alternative procedure [3] is to use quaternions to describe the rigid-body rotation about the body center of gravity G. The quaternion $\mathbf{q}$ arises from an ordered pair of a scalar s and a vector $\mathbf{v}$: $\mathbf{q} = (s, \mathbf{v})$ can be employed to describe rotations. A correspondence between rotations and quaternions is given by introducing the rotation quaternion is:

$$\mathbf{q} = \{\cos(\beta/2), \sin(\beta/2) \cdot \mathbf{u}\}$$

where β is the rotation angle and $\mathbf{u}$ identifies the rotation axis. Thus, expressing the rotation matrix $\mathbf{R}$ in terms of the components of the rotation quaternion, the set of Eq.1 is replaced, after some mathematics, by:

$$\begin{aligned} \dot{\mathbf{x}}_G &= \mathbf{v}_G \\ \dot{\mathbf{v}}_G &= \mathbf{f}/M \\ \dot{\mathbf{q}} &= 1/2\,\mathbf{Q}\{0, \omega_x, \omega_y, \omega_z\}^T \\ \dot{\boldsymbol{\omega}} &= \hat{\mathbf{J}}_b(\boldsymbol{\omega}) + \mathbf{J}_b^{-1}\mathbf{m} \end{aligned} \tag{2}$$

where the q_i's are the quaternion components, $\mathbf{Q}$ a matrix whose elements are the q_i's and $\hat{\mathbf{J}}_b$ is a proper vector. Since the quaternion representing a rotation has unit modulus, these four components are not independent and a normalization condition is added. Thus, a set of first-order differential equations is obtained in the unknown $\mathbf{y} = \{\mathbf{x}, \mathbf{v}, \mathbf{q}, \boldsymbol{\omega}\}^T$, directly available for numerical integration by a Runge-Kutta scheme. It is worth to note that it is not indeed the case of the equation $\mathbf{A}\ddot{\boldsymbol{\alpha}} + \mathbf{b} = \mathbf{m}$, needing the inverse of $\mathbf{A}$ that meets singularities.

Next, the force vector $\mathbf{f}$ (and $\mathbf{m}$) must be explicitly introduced in the previous set of equations. In particular, the vector $\mathbf{f}$ can be decomposed as:

$$\mathbf{f} = \mathbf{f}_{cab} + \mathbf{f}_b + \mathbf{f}_g + \mathbf{f}_{fl} \tag{3}$$

where $\mathbf{f}_{cab}$ is the cable force, $\mathbf{f}_b$ is the contact force exchanged by adjacent pontoons, $\mathbf{f}_{we}$ is the weight force and $\mathbf{f}_{fl}$ is the fluid force (in a similar way the vector of moments $\mathbf{m}$ can be also decomposed). The forces exerted by the fluid $\mathbf{f}_{fl}$ on the pontoons can be too decomposed as (see also [4]) $\mathbf{f}_{fl} = \mathbf{f}_{hs} + \mathbf{f}_m + \mathbf{f}_w$, with $\mathbf{f}_{hs}$ the hydrostatic force, $\mathbf{f}_m$ the force due to the body motion and $\mathbf{f}_w$ the wave force. In particular, the wave loads are determined by a first-order theory leading to the forces due to the incident waves. In this case, the expression of the force is

$$\mathbf{f}_w^{(1)} = Re\left(\sum_{j=1}^{N} \mathbf{H}(\omega_j, \mu)\zeta_{a,j} e^{i(\omega_j t + \epsilon_j)}\right)$$

where $\zeta_{a,j}$, ω_j, ϵ_j and μ are the wave-amplitude, the frequency, phase and heading angle, respectively. Because of the simple shape of the pontoons, the expression of the transfer function $\mathbf{H}(\omega_j, \mu)$ is provided in closed form (see [4]). The second-order wave loads have been also considered. Therefore, taking into account *(i)* the instantaneous position of both the body and the free-surface, and *(ii)* the nonlinearity associated with the velocity of the fluid particles, it is possible to include non-zero, slowly-varying, nonlinear mean forces in the form

$$\mathbf{f}_w^{(2)} = G(\omega_p)\,[\eta(t)]^2$$

where $\eta(t)$ is the wave-envelope, G is the wave spectrum, generally evaluated at the peak frequency ω_p and given by an expression due to Cox, $G = \rho g\, C^3 \sqrt{V}$, with $C = 0.35$ in the x direction and $C = 0.25$ in the y direction. Using a time-domain approach, the linearized Bernouilli theorem and under the hypothesis of non rotational fluid, Cummins [5] showed that the forces due to body motion can be expressed as:

$$\mathbf{f}_m = -\iint_{S_B} p \cdot \mathbf{n}\, dS = -\mathbf{A}\ddot{\mathbf{x}} - \int_{-\infty}^{t} \mathbf{B}(t-\tau)\dot{\mathbf{x}}\, d\tau$$

where $\mathbf{B}(t) = \frac{2}{\pi}\int_0^\infty \hat{\mathbf{B}}(\omega)\cos(\omega t)\, d\omega$ and $\mathbf{A} = \hat{\mathbf{A}}(\omega)|_{\omega=\infty}$, accordingly to Ogilvie, with $\hat{\mathbf{A}}$ and $\hat{\mathbf{B}}$ are the added mass matrix and the added damping matrix, respectively.

Finally, it can be remarked that the convolution integral can be evaluated by expressing the function $B(t)$ in terms of series of exponentials (Prony series, [6]), *i.e.*, $B(t) = \sum_{p=1}^{3} R_p e^{\lambda_p t}$, that after some algebra, allows to express the force at the time step $n+1$ in terms of the force at the previous time step n, *i.e.*, $f_p^{(n+1)} = e^{\lambda_p \Delta t} f_p^n - \frac{x^{n+1} - x^n}{\lambda_p \Delta t} R_p \left(1 - e^{\lambda_p \Delta t}\right)$ making the numerical scheme more effective and fast. The vector of body forces f_b exchanged between the pontoons is given both by shock forces - due to small collisions between the pontoons - and elastic forces due to the linking cables. Simple momentum and energy conservation are used to simulate occurrence of contact events between pontoons (cfr. [7]). The forces due to linking cables are in this case very simple since only taut configurations have to be considered and each linking cable collapses into a single spring element that does not supply any compression force. A rather general numerical model for the mooring-line forces is here introduced under the following hypotheses: *(i)* the material of the cable is isotropic, homogeneous and elastic; *(ii)* the displacements of points belonging to the same cross-section are identical; *(iii)* the previous choice about the displacement field implies that bending, torsion and shear stresses are neglected. This model is used for cables and chains as well. The following approach returns cable's equation of motion following an inverse way with respect to the usual one: a discrete - intuitive - model is developed, actually that used in the numerical code; corresponding nonlinear differential equa-

tions are determined when the size of the discrete element of the chain tends to zero. The advantage relies in a more clear physical meaning of the considered model. The continuous cable has its discrete counterpart approximation in a spring-mass chain of N elements. L is the length of the unloaded chain, giving Δs_0=$L/(N-1)$. Each element of the chain is replaced by a mass m=$\rho A_0 \Delta s_0$ and by a stiffness k=$EA_0/\Delta s_0$, where ρ, E, A_0 are the mass cable's density, elasticity modulus and cross-section area of the unloaded cable, respectively. The $i-$th mass equation is:

$$m\,\ddot{\mathbf{u}}_i = \mathbf{f}_i^{(+)} + \mathbf{f}_i^{(-)} + \mathbf{q}_i \Delta s_0 \qquad (4)$$

where $\mathbf{f}_i^{(+)}$ and $\mathbf{f}_i^{(-)}$ are the elastic forces applied by the adjacent elements, respectively, and $\mathbf{q}_i$ is the external load per unit length (including cable's weight, hydrostatic and drag forces, dissipation due to internal loss and friction between rings etc.). By using linear elastic constitutive relationship $\mathbf{f}_i^{(+)} = EA_0 \left\{ \left(|\Delta \mathbf{x}_i| / \Delta s_0 - 1 \right) \Delta \mathbf{x}_i / |\Delta \mathbf{x}_i| \right\}$, where $\Delta \mathbf{x}_i = \mathbf{x}_{i+1} - \mathbf{x}_i$ (a similar expression holds for $\mathbf{f}_i^{(-)}$), Eq. 4 is integrated with respect to the time variable by a Runge-Kutta fourth-order scheme. For $\Delta s_0 \to 0$, indicating with s is the curvilinear abscissa along the stretched cable configuration, Eq. 4 returns its continuous counterpart in the form:

$$\ddot{\mathbf{u}} = \frac{1}{c^2} \frac{\partial}{\partial s_0} \left[\left(\left| \frac{\partial \mathbf{x}}{\partial s_0} \right| - 1 \right) \frac{\partial \mathbf{x}}{\partial s} \right] + \frac{1}{\rho A_0} \mathbf{q}$$

where $c = \sqrt{E/\rho}$. Since $\partial \mathbf{x}/\partial s_0 = d\mathbf{x}_0/ds_0 + \partial \mathbf{u}/\partial s_0$, where $d\mathbf{x}/ds_0 = \boldsymbol{\tau}_0$ is the unit vector tangent to the reference cable's configuration, while $\partial \mathbf{x}/\partial s = \boldsymbol{\tau}$ is tangent to the actual cable configuration, one obtains:

$$\ddot{\mathbf{u}} = \frac{1}{c^2} \frac{\partial}{\partial s_0} \left[\left(\left| \boldsymbol{\tau}_0 + \frac{\partial \mathbf{u}}{\partial s_0} \right| - 1 \right) \boldsymbol{\tau} \right] + \frac{1}{\rho A_0} \mathbf{q}$$

that is the continuous cable equation corresponding to the numerical model given by Eq. 4. The nonlinearity arises both by the terms $\boldsymbol{\tau}$ and $\left| \boldsymbol{\tau}_0 + \frac{\partial \mathbf{u}}{\partial s_0} \right|$. When $\boldsymbol{\tau}$ is constant with respect to s, e.g. for a taut chain, and when $\partial \mathbf{u}/\partial s_0 << 1$, i.e. for small deformation, the previous equation returns the well known linear wave equation. Considering the tension T_i along the cable, given by $T_i = |\mathbf{f}_i^{(+)}| = EA_0 \left(|\Delta \mathbf{x}_i| / \Delta s_0 - 1 \right)$ (the section area is considered invariant), Eq. 4, for $\Delta s_0 \to 0$ becomes $\rho A_0 \ddot{\mathbf{u}} = \frac{\partial}{\partial s_0} (T \boldsymbol{\tau}) + \mathbf{q}$ In the case of chains the force along the line is slightly modified as follows:

$$\begin{cases} |\Delta \mathbf{x}_i| > \Delta s_0 & \Rightarrow \quad \mathbf{f}_i^{(+)} = EA_0 \left(\frac{|\Delta \mathbf{x}_i|}{\Delta s_0} - 1 \right) \Delta \mathbf{x}_i |\Delta \mathbf{x}_i| \\ |\Delta \mathbf{x}_i| < \Delta s_0 & \Rightarrow \quad \mathbf{f}_i^{(+)} = 0 \end{cases}$$

since compression forces are not supplied by the chain due to the unhooking between rings.

Let us analyse the added mass effect. The Morison's equation for a cylinder-shaped body states, accordingly to the potential theory, that the added mass effect depends on the acceleration normal to the cylinder axis. For an element Δs_0 of the cable, the corresponding added mass is $\mu\, \ddot{\mathbf{u}}_{norm} = \mu \left[\ddot{\mathbf{u}} - (\ddot{\mathbf{u}} \cdot \boldsymbol{\tau}) \boldsymbol{\tau} \right]$ that must be considered together with the cable's inertia term. Taking Eq. 4 with the added mass terms, it leads to:

$$\mathbf{M}_i \ddot{\mathbf{u}}_i = \mathbf{f}_i^{(+)} - \mathbf{f}_i^{(-)} + \mathbf{q}_i$$

where the mass matrix is not shown for sake of conciseness. The fluid-cable interaction forces are completed by the drag effect included through the formula (Triantafyllou, [8]) $\mathbf{f}_{drag} = c_n \mathbf{v}_n |\mathbf{v}_n| + c_t \mathbf{v}_t |\mathbf{v}_t|$ where $\mathbf{v}_n$ and $\mathbf{v}_t$ are the relative normal and tangent velocity of the fluid with respect to the cable and the c's suitable coefficients depending on the angle of attack of the fluid with respect to the local configuration of the cable. Finally, dissipation force along the cable are included in the model: viscous dissipation forces, simulating the internal loss of the material, and the friction forces due to the relative motion between adjacent rings. At the end each cable and each pontoon equations are coupled by imposing that the cable $N-th$ end element has the same co-ordinates of its attachment point at the pontoon.

4. EXPERIMENTAL RESULTS AND COMPARISON WITH NUMERICAL SIMULATIONS

Comparisons between numerical results and measurements of the body motion and cable forces are shown. The response of the floating structure was considered both in the case of deterministic (regular) and stochastic wave loads. Preliminary, a test carried out on a single freely-floating body is carried out by using non-zero initial conditions on heave, pitch and roll separately, aimed to contribute to the validation of the sea-keeping module of the numerical code. The comparison between experiments and simulations on heave is presented is presented in Fig. 3, showing a satisfactory agreement in terms of predicted frequency and amplitude decay rate is observed. The response of the

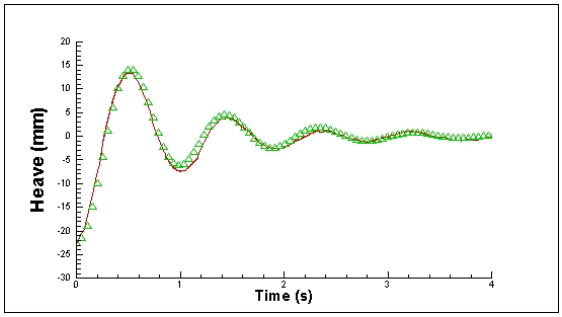

Figure 3: Free heave oscillations of a single pontoon.

whole floating structure undergoing regular wave loads is then considered. The wavelength has been chosen in order to excite the multi-body modes of vibration, whereas the wave amplitudes are reasonably small because this type of floating structure should be preferably moored in protected locations inside the harbors. During the tests the x-axis of the floating bodies is initially parallel to the wave direction and it oscillates in

the neighborhood of this mean position (yawing) being tied by the mooring lines. In Fig. 4 the time-history of heave is shown for the case of incoming waves with amplitude $a=4\ cm$, wavelength $\lambda_w=4/3\ L$ and frequency f_w=0.541 Hz. The agreement between simulations and tests is quite good both in amplitude and frequency (the two signals were numerically phased). This agreement is confirmed for pitch with wave amplitude $a=4\ cm$, wavelength $\lambda_w=L$ and frequency f_w=0.625 Hz.

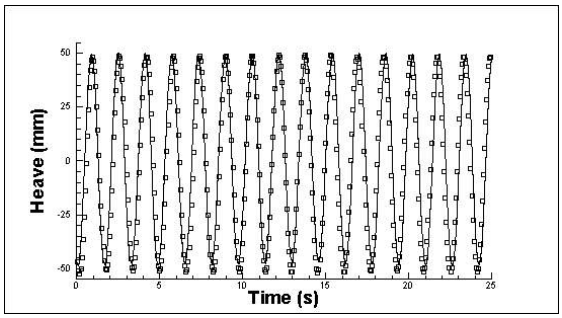

Figure 4: Heave response of pontoon n. 1.

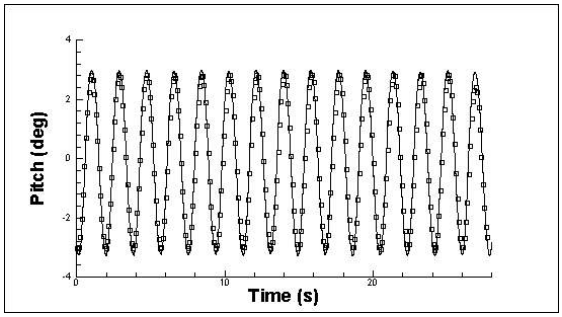

Figure 5: Pitch response of pontoon n. 1.

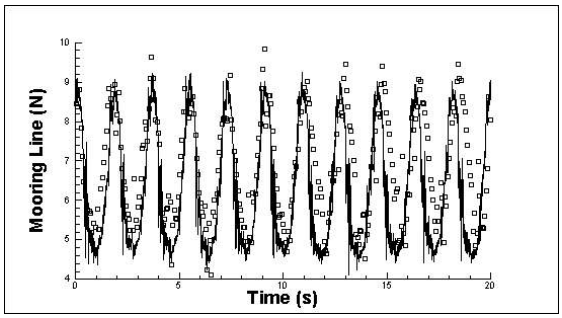

Figure 6: Left mooring line response of pontoon n.1.

In order to test the capability of the numerical code to deal with stochastic seaways, some tests were carried out with irregular waves generated through a Jonswap spectrum ($H_{1/3}=4\ cm$ and $T_1=1.6\ s$). Since, in this case, only a stochastically based comparison makes sense, the experimental statistical moments versus those obtained by the numerical simulations are given. Though the acquired signal lasts only 65 s, the agreement seems particularly satisfactory since the moments merge well up to the fourth-order (Experimental/Numerical, Standard Deviation: 7.10/7.27, Skewness: $-0.07/0.09$, Curtosis $-0.17/-0.28$).
The comparison between the recorded cable tension T and the numerical simulation for the case with incoming wave $a=4\ cm$, wavelength $\lambda_w=2\ L$ and frequency f_w=0.425 Hz is shown in Fig. 6. The general agreement seems good, both in terms of frequency and amplitude of the tension response. However, a general comment is needed concerning some local tension spikes in the experimental results not sharply shown by the numerical simulations. The case shows a single dominant frequency in the tension response that is correctly kept by the numerical model, but some spikes arise in the experiments that are not well reproduced by the numerical simulation. The experimental spikes (present also in other other tests not shown for sake of conciseness) arise when (a) the chain reaches the condition of ballast lifting, or (b) the spherical linkage connecting the cells to the pontoon reaches the maximum allowed angle, or (c) some of the front and the side chains of the pontoons intersect. Concerning the first point, the numerical code includes all the nonlinear effects due to the ballast lifting. This is the reason why also in the numerical simulations spikes arise. However, a well phased reproduction of the condition of ballast lifting implies that the chain initial configuration is exactly measured. It is clear how, although submerged cameras where used in positioning the dead bodies, it is not an easy task to reproduce exactly the configuration running on the numerical code. The effect mentioned at point b) is also included in the numerical model, but, again, it is extremely difficult to measure the initial chain orientation at the attachment point. Finally, the collision between chains is not numerically considered, although it seems not to be the more relevant effect in the spike generation.

ACKNOWLEDGEMENTS

This work was done in the frame of the Research Programme *"Programma Ricerca sulla Sicurezza"* funded by the *Ministero delle Infrastrutture e dei Trasporti*.

References

[1] Inoue, Y., Rafiqul, M. (2000)."Numerical Investigation of Slowly Varying Drift Forces of Multiple Floating Bodies in Short Crested Irregular Waves", *Proc. 10th ISOPE Conf.*.

[2] Ansari, K.A., Khan, N.U. (1986). "The effect of cable dynamics on the stationkeeping response of a moored offshore vessel", *Proc. 5th Int. OMAE Symp.*, ASME, Vol. III.

[3] Omelyan, I., (1999). "A new approach to the integration of rotational motion in systems with interacting rigid bodies", *J. Comput. Phys.*.

[4] Faltinsen, O. (1993). "Sea Loads on Offshore Structures", *Cambridge University Press*.

[5] Journee, J., Massie, W. (2001). "Offshore Hydromechanics ", *Delft University Press*.

[6] Osborne, M., Smyth, G. (1995). "A modified Prony Algoritm for Fitting Sums of Exponential Functions", *SIAM J. of Scientific Computing*, **16**.

[7] Lin, M. C. (1992)."Efficient Collision Detection for Animation and Robotics", *PhD Thesis, University of California, Berkley*.

[8] Triantafyllou, M. (1982)."Preliminary Design of Mooring System", *J. Ship Research*, **26**, No. 1.